Properties of AGN coronae in the *NuSTAR* era II: hybrid plasma

A.C. Fabian[1]∗, A. Lohfink[1], R. Belmont[2,3], J. Malzac[2,3] and P. Coppi[4]

[1] Institute of Astronomy, Madingley Road, Cambridge CB3 0HA
[2] Universite de Toulouse; UPS-OMP; IRAP; Toulouse, France
[3] CNRS; IRAP; 9 Av. colonel Roche, BP 44346, F-31028 Toulouse cedex 4, France
[4] Yale Center for Astronomy and Astrophysics, Yale University, New Haven, Connecticut 06520-8121, USA

25 January 2017

ABSTRACT
The corona, a hot cloud of electrons close to the centre of the accretion disc, produces the hard X-ray power-law continuum commonly seen in luminous Active Galactic Nuclei (AGN). The continuum has a high-energy turnover, typically in the range of one to several 100 keV and is suggestive of Comptonization by thermal electrons. We are studying hard X-ray spectra of AGN obtained with NuSTAR after correction for X-ray reflection and under the assumption that coronae are compact, being only a few gravitational radii in size as indicated by reflection and reverberation modelling. Compact coronae raise the possibility that the temperature is limited and indeed controlled by electron-positron pair production, as explored earlier (Paper I). Here we examine hybrid plasmas in which a mixture of thermal and nonthermal particles is present. Pair production from the nonthermal component reduces the temperature leading to a wider temperature range more consistent with observations.

Key words: black hole physics: accretion discs, X-rays: binaries, galaxies

1 INTRODUCTION

The primary power-law, X-ray emission from luminous accreting black holes originates from the corona, which is a hot cloud close to the centre of the accretion disc. Soft disc photons are Compton-upscattered in the corona to make the power-law continuum. It often shows a high-energy turnover somewhere between about 30 keV and 1 MeV, generally interpreted as the temperature of the corona (or a value close to it). The primary continuum is usually the most variable part of the spectrum, showing rapid changes which, when interpreted using X-ray reflection and reverberation signatures, indicate that the corona has a relatively small size of less than a few tens of gravitational radii ($r_g = GM/c^2$) (Fabian 2013; Reis & Miller 2013; Uttley et al. 2014). The fraction of the bolometric power passing through the corona ranges from about 10 to 50 per cent (Vasudevan & Fabian 2007).

A compact corona in a luminous accreting black hole system must be a dynamic structure since the heating and cooling timescales for the hot electrons are less than the light crossing time of the corona (Fabian et al. 2015, Paper I, F15). There is not enough time for any simple equilibrium to be established. This can be further considered by looking at the thermal energy content of the corona, which is small (Merloni & Fabian 2001, MF01). A spherical corona with typical properties of unit Thomson depth, $\tau_T = 1$, temperature $kT = 50\,\mathrm{keV}$ and radius $10R_1 r_g$ above a $10^6 m_6\,\mathrm{M_\odot}$

black hole has a very small mass of $M_c = 10^{-8}m_6^2 R_1^2\,\mathrm{M_\odot}$, thermal energy

$$E_{th} \approx 10^{42} m_6^2 R_1^2\,\mathrm{erg} \tag{1}$$

and crossing time $t_{cross} = 50 m_6 R_1$ s. The luminosity obtained if all the coronal energy is released on a crossing time $L_{cross} \approx 2 \times 10^{40} m_6 R_1\,\mathrm{erg\,s^{-1}}$ is much less than the Eddington luminosity L_{Edd}, in that $L_{cross}/L_{Edd} \approx 10^{-4}R_1$. Higher luminosities, as are typically observed, require that both cooling and heating occur on a faster timescale. As argued by MF01, the energy supplying the heat must be stored in the corona, probably in the form of magnetic fields powered by the accretion disc. It is then unclear, if only heating and cooling are involved, what controls the plasma temperature, or temperatures, in the corona and how any stable equilibrium is established.

Here we follow up on our recent paper (F15), which explored the properties (temperature and compactness) of coronae deduced in the light of *NuSTAR* observations. The coronal plasma is assumed to be thermal and the temperature at the maximum allowed by electron-positron pair production: heating pushes the temperature upward until it is balanced by the creation of pairs – the pair thermostat (Svensson 1984; Zdziarski 1985). *NuSTAR* observations of Active Galactic Nuclei (AGN) show they avoid the region where pair production runs away, indicating that the process may play a role. However there is a significant number of AGN for which the temperature is much smaller than expected on the basis of purely thermal pair production (e.g., Baloković et al. 2015; Ursini et al. 2016).

∗ E-mail: acf@ast.cam.ac.uk

Here we aim to tackle the issue of a low temperature corona by considering hybrid coronae containing a mixture of thermal and nonthermal particles. We assume that the corona is highly magnetized and powered by dissipation of magnetic energy. Such dissipation is often intermittent in both space and time. In a compact corona the heating and cooling are so intense that energetic particles may not have time to thermalize before inverse Compton cooling reduces their energy (see the electron-electron equilibration line in Fig. 1, which is adapted from F15: the electron-proton line lies about 3 orders of magnitude lower). Only a small fraction of the electrons need start from energies of an MeV or more for them to emit hard photons which collide and create electron-positron pairs. If the pairs are energetic enough then yet more pairs are produced and a runaway situation can occur. Meanwhile the cooled pairs can, before annihilating, share the available energy leading to a reduction in the mean energy per particle and thus temperature of the thermal population, which may be composed mostly of pairs. This can result in a relatively cool thermal particle population with a temperature well below 100 keV, a low-level hard tail and a possible broad annihilation line at 511 keV. Unless very sensitive hard X-ray observations are obtained, the emitted continuum appears to originate from a low-temperature thermal plasma incapable of pair production. Paradoxically, what appear to be the lowest temperature objects can be the most pair-dominated.

Hybrid models for the corona were introduced over two decades ago (Zdziarski, Lightman & Maciolek-Niedzwiecki 1993; Ghisellini, Haardt & Fabian 1993) providing a better explanation for the hard X-ray spectra of luminous accreting black holes than purely nonthermal (Svensson 1994) or thermal (Fabian 1994) models. Comparison of hybrid models with AGN spectra has been carried out on NGC4151 (Zdziarski, Johnson & Magdziarz 1996; Johnson et al. 1997), using OSSE data from the Compton Gamma-Ray Observatory to conclude that the nonthermal contribution in NGC4151 is less than 15 per cent. A study of stacked AGN spectra from OSSE by Gondek et al. (1996) was unable to distinguish between the possibilities. More recent work on NGC4151 using INTEGRAL data Lubinski et al. (2010) shows that thermal models fit the spectra, which extend up to 200 keV, in its bright state and that the source appears harder in its low state. There is no new information on any possible hard tail or annhilation feature; OSSE results remain the most sensitive at those energies. Integral spectra in the 2–200 keV band of 28 bright Seyfert galaxies, combined with lower energy data from other instruments, are characterized by thermal Componization with a mean temperature $kT \sim 50\,\mathrm{keV}$ (Lubiński et al. 2016) and a tail to higher values. We found a similar distribution from NuSTAR data (F15, Fig. 1).

Hybrid models have been successfully applied to the spectra of X-ray Black Hole Binaries (BHB) such as Cyg X-1 where high energy tails are clearly seen (Gierlinski et al. 1999; McConnell et al. 2001; Parker et al. 2015), for other sources see also (Grove et al. 1998; Kalemci et al. 2016; Wardzinski et al. 2002; Droulans et al. 2010). In this paper, we concentrate on AGN, since high-frequency, X-ray reverberation results indicate the location and size of the corona. Such reverberation has not yet been detected in BHB.

Our goal here is to compare the range of NuSTAR results with the pair thermostat operating in hybrid plasma. We are not at this stage attempting to reproduce spectra of individual objects. We define our parameters and discuss hybrid plasmas in more detail in Section 2. We compute and show $kT - \ell$ diagrams for various levels of the nonthermal fractional contribution. Finally we discuss our
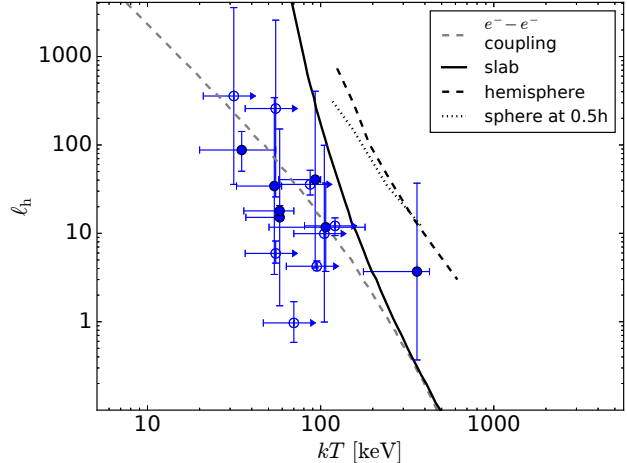
Figure 1. Electron temperature (kT) – compactness (ℓ) distribution for *NuSTAR* observed AGN (blue points) as first shown in Fabian et al. (2015). The e–e coupling line from Ghisellini, Haardt & Fabian (1993) is included: electrons in the region above the dashed line do not have time to thermally equilibrate with each other before cooling occurs. Pair lines, above and to the right of which there is runaway pair production, taken from Stern et al. (1995) are also shown. The slab line has been extrapolated slightly to higher ℓ. Open circles are used for objects where the temperature measurement is a lower limit. The temperatures shown are the observed values reported from spectral fits.
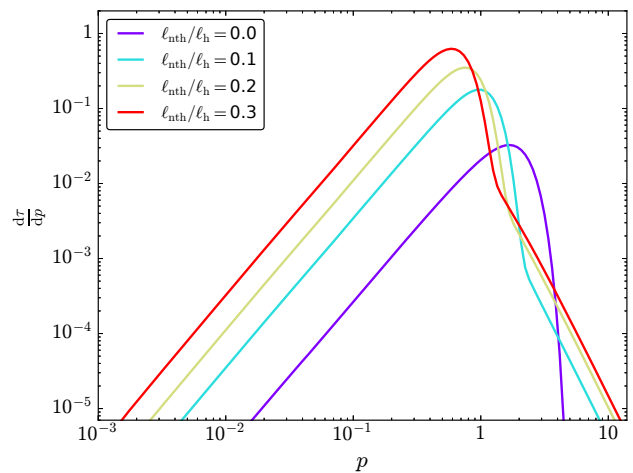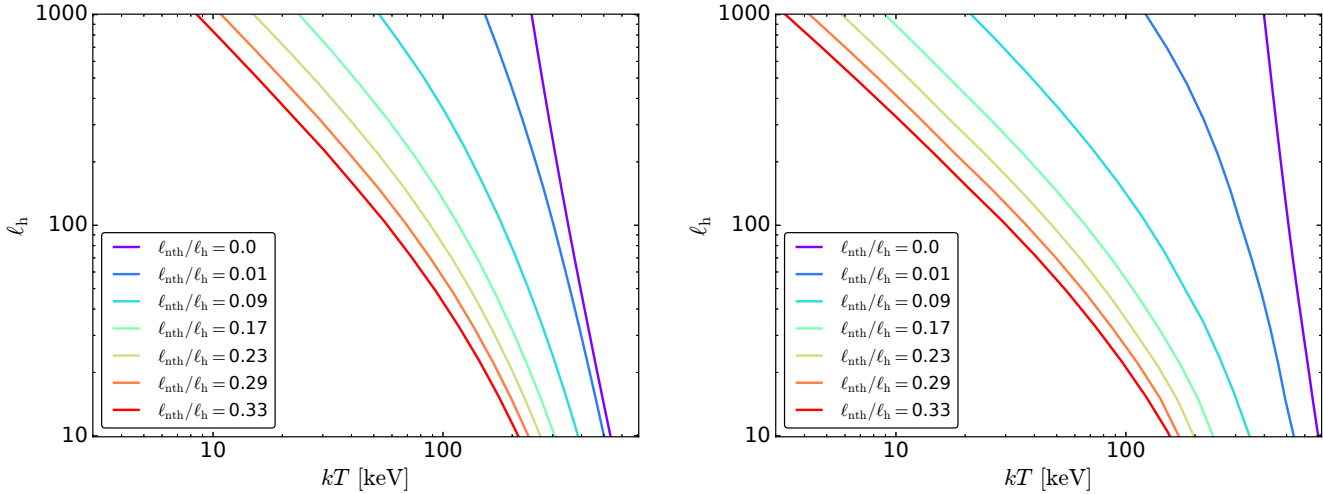

Figure 2. Lepton distributions for an increasing sequence of $\ell_{\mathrm{nth}}/\ell_{\mathrm{h}}$ and $\ell_h/\ell_s = 1$ at $\ell_{\mathrm{h}} = 100$, where p is the dimensionless lepton momentum ($\beta\gamma$) and $\frac{\mathrm{d}\tau}{\mathrm{d}p} = R \times \sigma_{\mathrm{T}} \times \frac{\mathrm{d}n}{\mathrm{d}p}$ with R being the radius of the sphere modelled by Belm, σ_{T} the Thomson cross-section, and n the lepton number density. As the non-thermal fraction increases the peak of the distribution moves to lower energies.

conclusions in Section 3. Detailed spectral comparison with individual objects is left to a later paper.

2   HYBRID PLASMAS

The excellent hard X-ray sensitivity of *NuSTAR* has allowed detailed spectral modelling of the reflection component and precise measurements of the spectral turnover in the continuum spectrum of many X-ray bright Active Galactic Nuclei (AGN) to be made.

Figure 3. $kT - \ell$ distributions for an increasing sequence of ℓ_{nth}/ℓ_h and two different ℓ_h/ℓ_s values: 1 (left panel), 0.1 (right panel). As the non-thermal fraction increases the equilibrium temperature is lower. Similarly, a geometry with more soft photons entering the corona leads to lower equilibrium temperatures.

In order to understand what sets those temperatures, it is useful to show these measurements in the form of a temperature-compactness, $kT - \ell$, diagram (Fig. 1; adapted from F15), where kT is the electron temperature and ℓ is the dimensionless compactness parameter

$$\ell = \frac{L}{R} \frac{\sigma_T}{m_e c^3} \qquad (2)$$

with L being the luminosity, R the radius of the source (assumed spherical), σ_T the Thomson cross section and m_e the mass of the electron.

Coronae should lie along one of the lines in the $kT - \ell$ plot, which in Fig. 1 represent the expectation for a purely thermal plasma, whose temperature is regulated by pairs. This takes place as the corona is heated and driven diagonally upwards from left to right in the plot (i.e. increasing both L and kT) until pairs start to form from energetic collisions. This then reduces and finally stabilizes the temperature at the line.

Sources should not be seen to the right of the line, since catastrophic pair production would ensue, rapidly driving down the temperature. If a source is confirmed to occur and remain in the forbidden region, then the basis of the model needs to be re-considered, with something other than a static compact corona being relevant. Jetted emission would be more likely in this case. Objects well to the left of the line pose the problem of what stabilizes them in such a highly dynamic situation?

We propose here that hybrid coronae can solve this problem. In our hybrid corona scenario, we assume that part of the coronal heating power, L_{nth}, creates a nonthermal power-law electron spectrum within the source, with compactness parameter ℓ_{nth}. The thermal heating of the electron population ℓ_{th} and the injection of soft photons ℓ_s continues as in a standard, thermal scenario. The total heating is then given by $\ell_h = \ell_{th} + \ell_{nth}$ and the nonthermal fraction is thus ℓ_{nth}/ℓ_h. The ratio ℓ_h/ℓ_s, together with the Thomson optical depth τ, plays a strong role in determining the power-law slope of the emerging X-ray radiation, with high values leading to a flat spectrum and low values to a steep one. Increasing τ, which can be a result of pair production, tends to harden the spectrum.

We use the BELM code (Belmont, Malzac & Marcowith 2008) for simulating emission from hybrid plasmas. (Comparable
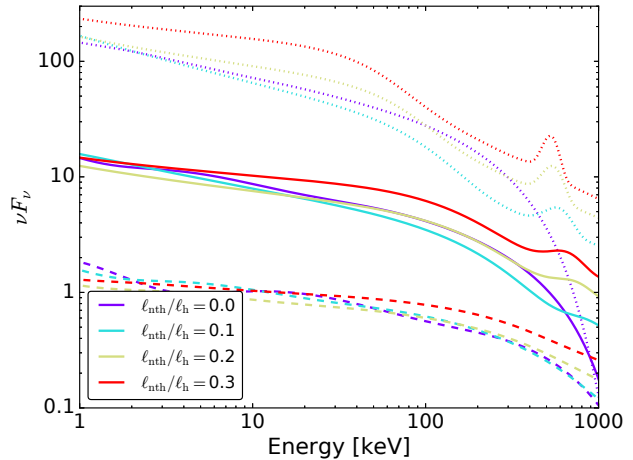
Figure 4. Simulated spectra for ℓ_h of 10, 100, 1000 (dashed, solid, dotted) and ℓ_h/ℓ_s of 1 for an increasing sequence of ℓ_{nth}/ℓ_h.

results are obtained using EQPAIR[1] (Coppi 1999).) BELM simultaneously solves the coupled kinetic equations for leptons and photons in a (magnetized,) uniform, isotropic medium. The equilibrium energy distributions of the Comptonizing leptons are calculated self-consistently, taking into account the coupling between particles and radiation. Radiation transfer is dealt with using a simple escape probability formalism. The code takes into account all the relevant radiation processes such as self-absorbed synchrotron radiation, Compton scattering, self-absorbed bremsstrahlung radiation, pair production/annihilation, coulomb collisions, and uses prescriptions for particle heating/acceleration. In the simulations shown in this paper the effects of cyclo-synchrotron radiation are neglected (magnetic field is set to 0 G). EQPAIR is very similar (and gives identical results) but assumes the low energy component of the electron distribution is a perfect Maxwellian, while our electron distributions are calculated according to the full kinetic equa-

---
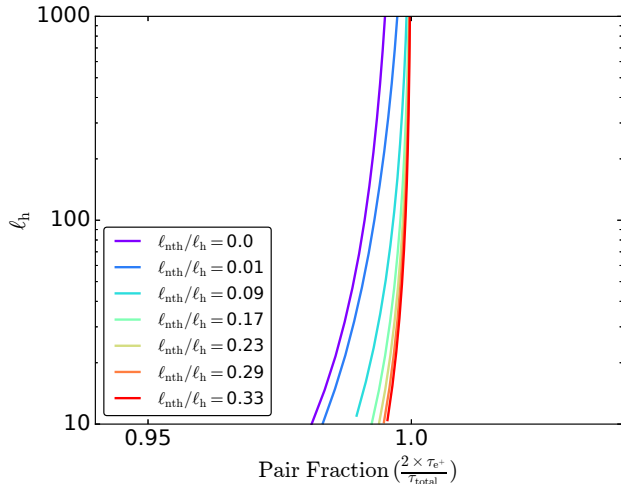
Figure 5. Pair fraction for an increasing sequence of $\ell_{\mathrm{nth}}/\ell_{\mathrm{h}}$ and $\ell_h/\ell_s = 1$. While the corona can be considered pair dominated for all cases, the pair fraction increases further for a higher non-thermal contribution.

Figure 6. *NuSTAR* data overplotted on the theoretical predictions for $kT - \ell$ distributions for an increasing sequence of $\ell_{\mathrm{nth}}/\ell_{\mathrm{h}}$ with $\ell_{\mathrm{h}}/\ell_{\mathrm{s}} = 1$. The data have been corrected for gravitational redshift.

tions in BELM. Non-thermal particles are injected with a power-law index of 2.5 ranging from $\gamma_1 = 1.3$ to $\gamma_2 = 1000$ for the purpose of this paper.

The electron temperature is obtained by fitting the thermal part of the lepton distribution with a Maxwellian. While this approximation becomes less accurate as the non-thermal contribution to the lepton distribution increases (Fig. 2), it still characterizes the general behavior of the temperature well.
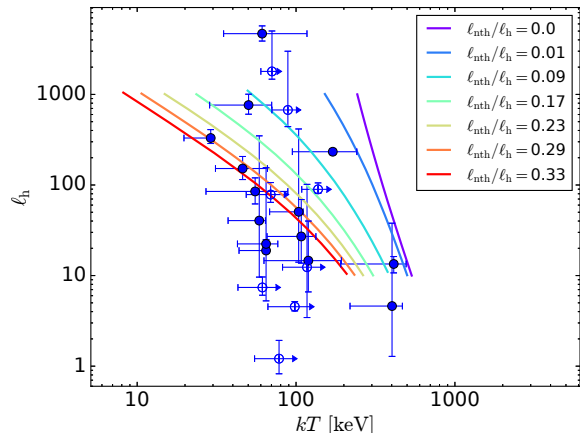
Figs 3 show the $kT - \ell$ distribution as lines at constant values of $\ell_{\mathrm{nth}}/\ell_{\mathrm{h}}$ and for two different values (1 and 0.1) of ℓ_h/ℓ_s. Hard X-ray spectra for a fixed ratio of $\ell_{\mathrm{th}} = 100$ and an increasing sequence of $\ell_{\mathrm{nth}}/\ell_{\mathrm{h}}$ are shown in Fig. 4. We see that as the nonthermal power is increased from zero, then the temperature of the thermal component drops from around several hundred keV to below 20 keV. The drop in spectral turnover is apparent in the spectra as is the rise of the hard X-ray flux and the annihilation line at the highest nonthermal fractions.

To assure ourselves that the observed decrease in electron temperature is due to pairs we plot the pair fraction in Fig 5. It is clear that the coronae are pair dominated.

Finally, in Fig. 6 we show the *NuSTAR* data points from Fig. 1 again in the $kT - \ell$ diagram with our hybrid corona results overlaid. A few new data points have been added from very recent results, see Table 1 for details. The new values were obtained in a similar fashion to Fabian et al. (2015). In contrast to Fig. 1, we corrected the datapoints for gravitational redshifting assuming the measured coronal size and height given in Table 1 or $10r_{\mathrm{g}}$ if no measurement exists. A 10 to 30 per cent nonthermal contribution appears sufficient to account for most of these objects and particularly those with well constrained temperatures.

We have not accounted for the effect of light bending on coronal flux as this depends on the inclination and other parameters. It could increase the intrinsic value of ℓ_h by a factor of two, or even more if the corona lies close to the black hole. If the emission site within the corona is very localized then the observationally inferred value of ℓ_h could be underestimated by a factor of a few.

We note that most of the spectral fits used in determining the coronal temperatures assume a power-law continuum with an exponential high-energy cutoff as an approximation to a full Comptonization spectrum. This introduces a systematic uncertainty in the temperature, since the cutoff energy is 2–3 times higher than the gas temperature depending on the optical depth of the corona (i.e whether thin or thick) and also on the geometry of the corona and its illumination (see e.g. Petrucci et al. 2001).

3   DISCUSSION

We find that current data are consistent with the pair thermostat operating and determining the temperature of compact AGN coronae, provided that a hybrid plasma is involved. For most sources, only a small addition of nonthermal plasma is required. The wide range of temperatures at a fixed value of ℓ_h can be accounted for with a non-thermal fraction ranging up to 30 per cent. Objects measured to have the lowest temperatures require the greatest nonthermal fraction. They should then have the strongest high energy tail and broad annihilation lines. Such features are generally undetectable with present instrumentation in AGN.

We also acknowledge that the simple one zone approach in the current modelling is probably too simplistic to capture the likely geometry of the corona and introduces a small uncertainty in the predicted temperatures.

In future work, we shall explore the location of individual sources in $kT - \ell_{\mathrm{h}} - \ell_{\mathrm{h}}/\ell_{\mathrm{s}}$ space, which plays a role in determining the spectral index as well as the continuum cutoff. We shall also include Stellar Mass Black Hole Binaries (BHB) and investigate the effect of magnetic fields acting through the synchrotron boiler (see e,g. Malzac & Belmont (2009); Veledina, Vurm & Poutanen (2011)) on current spectral results.

REFERENCES

Baloković M. et al., 2015, ApJ, 800, 62

Belmont R., Malzac J., Marcowith A., 2008, A&A, 491, 617

Bentz M. C., Walsh J. L., Barth A. J., 2010, ApJ, 716, 993

Coppi P. S., 1999, High Energy Processes in Accreting Black Holes

Droulans R., Belmont R., Malzac J., Jourdain E., 2010, ApJ, 717, 1022

Fabian A. C., 1994, ApJS, 92, 555

Fabian A. C., 2013, in IAU Symposium, Vol. 290, Feeding Compact Objects: Accretion on All Scales, Zhang C. M., Belloni T., Méndez M., Zhang S. N., eds., pp. 3–12

Fabian A. C., Lohfink A., Kara E., Parker M. L., Vasudevan R., Reynolds C. S., 2015, MNRAS, 451, 4375

Fuerst F., Mueller C., Madsen K. K., Lanz L., 2015, ApJ, 819, 13

Ghisellini G., Haardt F., Fabian A. C., 1993, MNRAS, 263

Gierlinski M., Zdziarski A. A., Poutanen J., Coppi P. S., Ebisawa K., Johnson W. N., 1999, MNRAS, 309, 496

Gondek D., Zdziarski A. A., Johnson W. N., George I. M., McNaron-Brown K., Magdziarz P., Smith D., Gruber E., 1996, MNRAS, 282, 646

Grier C. J. et al., 2013, ApJ, 773, 90

Grier C. J. et al., 2012, ApJ, 755, 16

Grove J. E., Johnson W. N., Kroeger R. A., McNaron-Brown K., Skibo J. G., Phlips B. F., 1998, ApJ, 500, 899

Johnson W. N., McNaron-Brown K., Kurfess J. D., Zdziarski A. A., Magdziarz P., Gehrels N., 1997, ApJ, 482, 173

Kalemci E., Begelman M. C., Maccarone T. J., Dincer T., Russell T. D., Bailyn C., Tomsick J. A., 2016, MNRAS, 463, 615

Lanzuisi G., Perna M., Comastri A., Cappi M., Dadina M., 2016, Astronomy & Astrophysics, 590, 12

Lubiński P. et al., 2016, MNRAS, 458, 2454

Lubinski P., Zdziarski A. A., Walter R., Paltani S., Beckmann V., Soldi S., Ferrigno C., Courvoisier T. J. L., 2010, MNRAS, 408, 1851

Madsen K. K. et al., 2015, ApJ, 812, 14

Malzac J., Belmont R., 2009, MNRAS, 392, 570

McConnell M. L. et al., 2001, ApJ, 572, 984

Merloni A., Fabian A. C., 2001, MNRAS, 321, 549

Neumayer N., Cappellari M., Reunanen J., Rix H. W., van der Werf P. P., de Zeeuw P. T., Davies R. I., 2007, ApJ, 671, 1329

Parker M. L. et al., 2015, ApJ, 808

Peterson B. M. et al., 2005, ApJ, 632, 799

Peterson B. M. et al., 2004, ApJ, 613, 682

Petrucci P. O. et al., 2001, ApJ, 556, 716

Reis R. C., Miller J. M., 2013, ApJ, 769, L7

Stern B. E., Poutanen J., Svensson R., Sikora M., Begelman M. C., 1995, ApJ, 449, 13

Svensson R., 1984, MNRAS, 209, 175

Svensson R., 1994, ApJS, 92, 585

Trevese D., Perna M., Vagnetti F., Saturni F. G., Dadina M., 2014, ApJ, 795, 9

Ursini F. et al., 2016, MNRAS, 463, 382

Uttley P., Cackett E. M., Fabian A. C., Kara E., Wilkins D. R., 2014, The A&A Review, 22, 72

Vasudevan R. V., Fabian A. C., 2007, MNRAS, 381, 1235

Veledina A., Vurm I., Poutanen J., 2011, MNRAS, 414, 3330

Wardzinski G., Zdziarski A. A., Gierlinski M., Grove J. E., Jahoda K., Johnson W. N., 2002, MNRAS, 337, 829

Woo J., Urry C. M., 2002, ApJ, 579, 530

Zdziarski A. A., 1985, ApJ, 289, 514

Zdziarski A. A., Johnson W. N., Magdziarz P., 1996, MNRAS, 283, 193

Zdziarski A. A., Lightman A. P., Maciolek-Niedzwiecki A., 1993, ApJ, 414, L93

Zoghbi A. et al., 2015, ApJL, 799, 5

Table 1. The targets and properties of the active galactic nuclei with cut-off constraints resulting from observations with *NuSTAR*. The references to the individual works are given in the right-most column.

Source	z	log(M) [$M_\odot$]	$r_{\rm co}$ [r_G]	F_x	$E_{\rm cut}$ [keV]	kT	ℓ	$(1+z_{\rm grav})$	Γ	Data	References
Cen A	0.002	$7.65^{+0.11}_{-0.14}$	10	34.34	>1000	>333	11^{+4}_{-3}	1.12	1.80 ± 0.01	XMM/NU	$1-2$
NGC 4593	0.009	$5.45^{+0.13}_{-0.15}$	10	0.50	90^{+40}_{-20}	45^{+20}_{-22}	612^{+242}_{-158}	1.12	$1.59^{+0.03}_{-0.02}$	XMM/NU	$3-4$
Mrk 766	0.013	$6.8^{+0.05}_{-0.06}$	3.4	0.88	>441	>147	244^{+34}_{-27}	1.48	$2.22^{+0.02}_{-0.03}$	XMM/NU	$5-6$
3C 120	0.033	7.75 ± 0.04	10	2.23	305^{+142}_{-74}	153^{+71}_{-76}	153^{+18}_{-16}	1.12	$1.70^{+0.10}_{-0.03}$	XMM/NU	$7-8$
PG 1211+143	0.081	$8.16^{+0.11}_{-0.16}$	10	0.32	>124	>41	63^{+28}_{-14}	1.12	2.51 ± 0.2	NU	$9-10$
4C 74.26	0.104	9.6 ± 0.5	7	1.17	183^{+51}_{-35}	92^{+26}_{-42}	20^{+42}_{-13}	1.18	1.81 ± 0.03	Swift/NU	$11-12$
3C 273	0.158	$8.84^{+0.16}_{-0.11}$	10	1.71	52^{+2}_{-2}	26^{+1}_{-9}	365^{+79}_{-43}	1.12	1.66 ± 0.01	NU	$13-14$
PG 1247+267	2.038	$8.3^{+0.17}_{-0.15}$	4	0.02	89^{+134}_{-34}	45^{+56}_{-26}	2480^{+1023}_{-803}	1.38	$2.35^{+0.09}_{-0.08}$	XMM/NU	$15-16$
53^{+2}_{-2}	XX	XX	XMM/NU	$17-18$							

F_x is the 0.1-200 keV X-ray flux in $10^{-10}\,{\rm erg\,cm^{-2}\,s^{-1}}$.

References: 1: Fuerst et al. (2015), 2: Neumayer et al. (2007), 3: Ursini et al. (2016), 4: Peterson et al. (2005), 5: Buisson et al., in prep., 6: Bentz, Walsh & Barth (2010),Grier et al. (2013), 7: Lohfink et al., in prep., 8: Grier et al. (2012), 9: Zoghbi et al. (2015), 10: Peterson et al. (2004), 11: Lohfink et al., submitted, 12: Woo & Urry (2002), 13: Madsen et al. (2015), 14: Peterson et al. (2004), 15: Lanzuisi et al. (2016) ,16: Trevese et al. (2014)